ELSEVIER

Contents lists available at ScienceDirect

International Journal of Mass Spectrometry

journal homepage: www.elsevier.com/locate/ijms





A simplified coaxial ion trap mass analyzer: Characterization of the simplified toroidal ion trap with a rectilinear ion guide

David V. Sirbescu-Stanley^a, Kristina M. Lemmer^a, Daniel E. Austin^b, Nicholas R. Taylor^{a,*}

- ^a Department of Mechanical and Aerospace Engineering, Western Michigan University, Kalamazoo, MI, USA
- b Department of Chemistry and Biochemistry, Brigham Young University, Provo, UT, USA

ARTICLE INFO

Keywords:
Rectilinear ion guide
Toroidal ion trap
Coaxial ion trap
Trapping capacity
Trapping efficiency
Selective mass ejection

ABSTRACT

A new miniature coaxial ion trap mass analyzer with a rectilinear ion guide has been constructed using a combination of planar and cylindrical electrodes. The results reported here focus on characterizing the performance of the rectilinear ion guide and simplified toroidal ion trap components. The simplified toroidal ion trap was found to have an ion capacity in excess of 10^5 ions and mass spectral resolution of 0.5–0.6 when used as a mass analyzer. The ion storage efficiency within the toroidal trapping region was evaluated and found the stored ion population decreased exponentially with storage time. Ion losses depended slightly on the stored β_z condition. Ion losses within the toroidal region are attributed primarily to field instabilities at the intersection point of the two components while charge exchange reactions were observed but considered a minor loss mechanism. The ability to mass selectively ejection ions of a specific mass from the toroidal trapping region was characterized and found to approach 100 % efficiency under appropriate ejection conditions.

1. Introduction

In 1953 Wolfgang Paul introduced the first quadrupole ion trap (QIT) and inspired a new branch of mass spectrometry [1]. Since the introduction of this novel device little has changed from its original design with stretching the end caps for increased analytical performance being the one notable exception [2]. The standard QIT used in modern mass spectrometers is simple in design and is composed of a hyperbolic ring electrode with a typical inner radius of 1.0 cm and two hyperbolic end caps. The application of a radio-frequency (RF) potential ($\sim\!15~kV_{pp}$) to the ring electrode generates the field required to focus ions to the center of the trapping region.

Ion dynamics and stability within the trapping region are predicted using the well-known Mathieu equation and associated Mathieu parameters [3,4]. An interesting aspect of the Mathieu parameters are the quadratic relationship between the physical dimensions of the trap and RF voltage required to eject an ion for analysis; thus, large power savings can be realized by reducing the physical dimensions of the trap. Reduced trapping dimensions also decreases the amplitude of ion oscillation for a given secular frequency. As a result, ions experience fewer buffer gas collisions with reduced kinetic energy per collision. Therefore, an ion trap with reduced physical dimensions can operate at higher relative

pressures, allowing smaller, low-power pumps to be utilized. These design advantages have since been leveraged in the development of miniaturized devices for the purpose of field portable chemical analysis. Unfortunately, the fabrication of hyperbolic electrodes on the millimeter scale with acceptable dimensional tolerances proved to be very challenging, imposing a scale limit on the miniaturization of QIT devices. Moreover, reduced trapping dimensions also imposed a performance limit, with space charge repulsion effects greatly reducing the ion trapping capacity resulting in degraded analytical performance. Solutions to these fabrication and space charge issues were found by altering the QIT electrode design. It was discovered that ion capacity could be significantly increased by extending the dimensionality of the device; therefore, the linear ion trap (LIT) and toroidal ion trap (TorIT) were invented [5,6]. These devices greatly increased the dimensionality of the characteristic trapping region, allowing a significantly larger bulk ion population to be stored within the device prior to detection. The increased number of detectable ions also had a \sqrt{N} signal-to-noise ratio (SNR) advantage, with N equal to the number of detected ions. A solution to the fabrication issue was achieved by simplifying the electrode design with cylindrical and planar electrodes replacing the more challenging hyperbolic electrodes. The combination of these two electrode design modifications have led to the creation of the cylindrical ion trap

E-mail address: Nicholas.taylor@wmich.edu (N.R. Taylor).

^{*} Corresponding author.

(CIT), rectilinear ion trap (RIT), and simplified toroidal ion trap (STorIT) [7–9]. An interesting aspect of RIT and STorIT designs is the decoupling of the characteristic trapping dimension and the trapping capacity of the device. As a result, these devices can be significantly miniaturized while maintaining an acceptable trapping capacity by simply increasing the aspect ratio of the device. Experimental and simulation studies examining the impact of various electrode designs on the performance of RIT, TorIT, STorIT, and related systems have been thoroughly examined [8–24]. As a result, the RIT and STorIT devices are ideal for miniaturization and inclusion into field portable chemical analysis systems.

Unique miniature ion traps using non-equipotential electrodes have also been researched. Work conducted in Austin's group has reported on the use of thin metal electrodes lithographically patterned onto two parallel ceramic plates [25–30]. These devices allowed the electric field to be modified in real time by adjusting the potential applied to each individual electrode within the device. This novel approach allowed various trapping dimensions to be realized including a QIT (Paul), TorIT (Halo), LIT, and the first reported example of a coaxial ion trap. With respect to the coaxial ion trap, the electric fields were adjusted to generated an outer TorIT trapping region and a central QIT. Unfortunately, mass selective ejection from the TorIT region into the QIT region could not be demonstrated [30].

An interesting aspect of the STorIT design reported by Taylor and Austin is found in the hollow cavity created due to the electrode design [9]. This configuration is ideal for the development of a coaxial trap, where a CIT can be created within a STorIT resulting in a simplified coaxial ion trap (SCIT) design. The advantage the SCIT design is realized with the ability to sample and analyze a range of masses stored within the high capacity STorIT region. Ions of a specific mass can be selectively transferred from the bulk ion population via resonance ejection into the CIT where tandem mass analysis (MS²) can be conducted, providing a distinct analytical advantage. The resonant ion transfer and subsequent MS² analysis can be repeated for a range of specific masses trapped within the STorIT, greatly increasing sample utilization efficiency. This attribute can be especially important in systems with limited sample quantities.

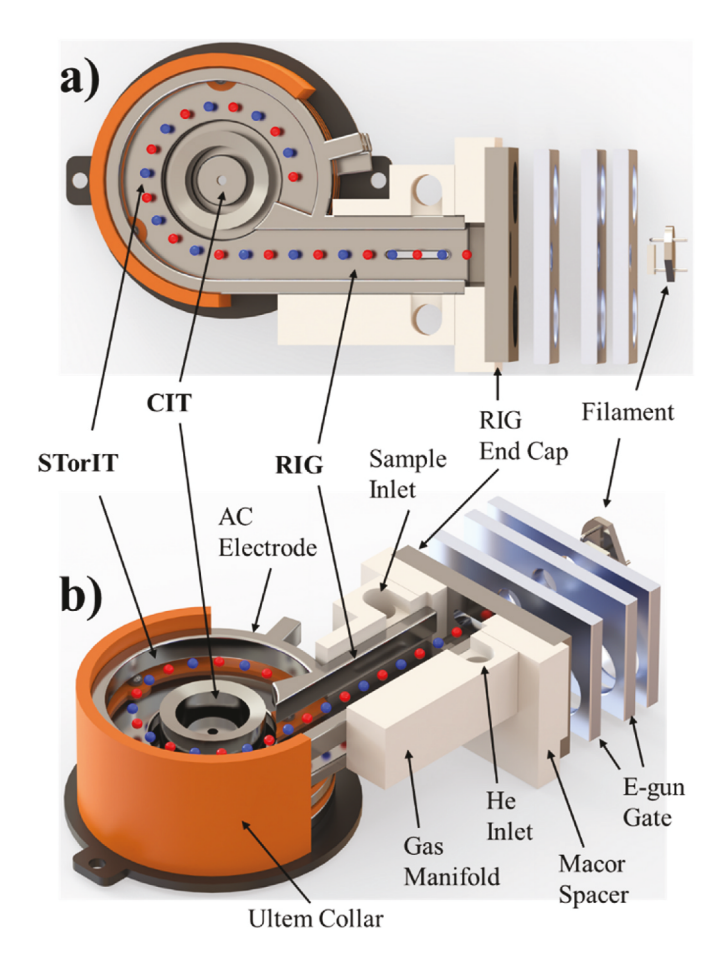
Recently, Gamage et al. reported a simulation study focused on the electrode geometry, electric field composition, and performance of a SCIT [31]. They demonstrated ions could be mass selectively transferred from a STorIT region and captured by a CIT when the proper relative RF phase angle between the two traps was utilized. The work presented here builds on the optimized design reported by Gamage et al. with the first experimental evaluation of a constructed SCIT mass analyzer with an aspect ratio of 3 [31]. The fabricated SCIT was also designed with a rectilinear ion guide (RIG) which tangentially intersects the STorIT. While ions could be generated directly within the STorIT region as reported by Taylor and Austin [9], the inclusion of a RIG component facilitates the injection of externally generated ions via electrospray, paper spray, laser-based, or plasma-based ionization methods. Therefore, the formation of a miniature ion trap device composed of RIG, STorIT, and CIT components yields a versatile analytical device for portable chemical analysis.

Since experimental functionality of the current prototype SCIT has not been previously reported, it is imperative to begin with the experimental evaluation of the RIG and STorIT components. Therefore, the work presented here will evaluate the RIG and STorIT's ion trapping capacity, ion storage efficiency, mass resolution, and ability of the STorIT to efficiently and selectively eject ions of a desired mass. The results reported here, including operational parameters, are necessary for future studies focused on the operation and interpretation of experimental data obtained from a fully assembled SCIT device.

2. Experimental design

2.1. Electrode design

The fabricated SCIT consisted of seven stacked electrodes designed to form the RIG, STorIT, and CIT components: top and bottom CIT end caps, top and bottom CIT barrels, top and bottom STorIT RF $_{Tor}$ electrodes, and a central AC $_{Tor}$ electrode. A cross-sectional rendered CAD image of the constructed system is shown in Fig. 1a with associated components identified. A cross-sectional illustration of the STorIT and



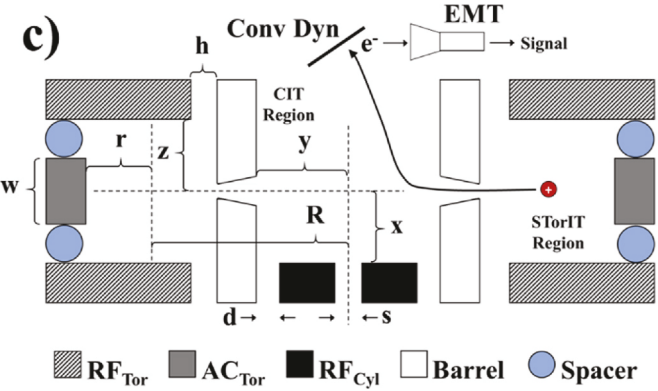


Fig. 1. a) A cross sectional rendered CAD image (top view) of the constructed SCIT with components labeled. b) Same as in a) with an angled view with components labeled. The red and blue spheres represent trapped ions. c) Cross sectional illustration of the STorIT and CIT trapping regions with the top CIT end cap removed. Dimensions: r=5.0 mm, w=5.0 mm, v=5.5 mm. Aspect ratio (R/r) = 3.

CIT trapping regions are shown in Fig. 1b with electrodes and dimensions noted. All electrodes were machined from 304 stainless-steel with tolerances ± 0.001 ". Spacing between electrodes was achieved using silicon nitride (SiN) ceramic ball bearings (OrTech Inc, Sacramento, CA). These spacers have a diameter tolerance of ± 0.00005 ", which provides excellent electrode spacing accuracy. As noted, the primary goal of this study is to evaluate the performance of the RIG and STorIT components; therefore, the top CIT end cap electrode was removed, allowing ejected ions to be directly detected. The STorIT and CIT electrodes were aligned with an Ultem collar. The RIG electrode alignment was achieved with a precision machined Macor spacer between the RIG end cap and RIG trapping electrodes.

Initially, SIMION simulations were used to optimize the design of the SCIT electrodes. The initial design involved using an AC_{Tor} electrode geometry which created a complete toroidal trapping region. Unfortunately, our initial simulation effort found the transfer of ions from the RIG region into the STorIT region was very inefficient, with a large population of ions scattering out of the trapping volume as they crossed the RIG-STorIT intersection point. To alleviate this issue and enhance the ion transfer efficiency from the RIG into the STorIT region, the geometry of the AC_{Tor} electrode was redesigned to its current geometry which provided a smoother field transition between the RIG and STorIT trapping regions, as shown in Fig. 1a. While this new design truncates the toroidal trapping region, the small loss in ion signal from the toroidal trapping region now occupied by the modified AC_{Tor} electrode is more than offset by a near 100 % transmission efficiency achieved between the two trapping regions.

A high Q-head power supply (PSRF-151, Adara Technologies, Adara, PA) was used to supply the RF potential to the STorIT electrodes. Control of the RF amplitude was achieved with an RF power controller (PSRF-125, Adara Technologies, Adara, PA) and an arbitrary waveform generator (33500B, Keysight, Colorado Springs, CO). Low-voltage power supplies (SPD 3303X-E, SIGLENT Technologies, Solon, OH) were used to provide the DC offset to the RF waveform and DC potential to the RIG end cap. A second function generator (33500B, Keysight, Colorado Springs, CO) supplied the AC and DC potentials to the AC $_{\rm Tor}$ electrode for resonance ejection. A small positive DC potential was applied to the bottom CIT end cap (PS310, Stanford Research Systems, Palo Alto, CA) to aid in directing ions towards the detection system as will be discussed below. The CIT barrel electrodes were grounded.

2.2. Vacuum chamber and gas handling system

The vacuum chamber consisted of an 8.0-inch to 6.0-inch conflat reducing tee. A turbomolecular pump (Turbovac SL 80H, Leybold, Export, PA) was attached to the 6.0-inch flange and backed with a dry scroll pump (Scrollvac SC 5 D, Leybold, Export, PA). Pump-down times of approximately 24 h would typically yield a chamber pressure $\leq\!1.0$ $\mu\text{Torr}.$ The ion trap assembly was mounted to the front 8-inch conflat flange while gas and power inlets were coupled into the chamber from the back 8-inch conflat flange with appropriate feedthroughs.

Chromatographic grade helium (HE CH300, Airgas, Radnor, PA) was used as the buffer gas and was supplied to the system with a calibrated mass flow controller (SmartTrak 50, Sierra Instruments, Monterey, CA) which allowed precise buffer gas pressure control within the RIG and STorIT regions. The helium buffer gas and analyte vapors used throughout this study were introduced directly into the RIG ionization region using a custom fabricated Macor gas manifold as shown in Fig. 1a. In addition, the helium supply line within the vacuum system was split in order to uniformly supply helium to both the RIG and STorIT regions. The partial pressure of all gas samples examined within this study were controlled with a leak valve (Model 203, Granville Phillips). Pressures within the STorIT were measured with a Pirani gauge (CVG101 Worker Bee, InstruTech, Longmont, CO) while the vacuum chamber pressure was measured with a cold cathode gauge (PTR90RN, Leybold, Export, PA). Helium buffer gas pressure of 1.5 mTorr and

sample pressures of 5 $\mu Torr$ were typically used throughout this work unless otherwise noted. Under these conditions, the vacuum chamber was able to maintain a pressure ${\sim}50~\mu Torr$ and was suitable for the presented work.

2.3. Ionization system

Ionization was achieved with an electron gun (E-gun) constructed with a thermionic filament (03-920437-00, Adaptas Solutions, Palmer, MA) mounted to a custom machined Macor frame. The filament was powered by a filament controller (Model 160, ArdaraTech, Adara, PA) capable of varying the electron energy and emission current. An electron energy of 70 eV was used throughout this study. The electron beam was directed through four aluminum electrodes with the first electrode grounded, the central two electrodes used to gate the beam with a high voltage single pole double throw reed relay (BFH-1C-05E, Comus International, Clifton, NJ) and the RIG end cap used as the final electrode. The response time of the relay limited reliable ionization gates to a minimum 5 ms. The aluminum electrodes noted in Fig. 1a were designed in an Einzel lens configuration for future studies examining the focusing and injection of externally generated ions into the RIG region. For the work reported here, the E-gun assembly was positioned to inject electrons through the RIG end cap slit and coaxial with the trapping region and gas introduction system.

2.4. Detection system

As discussed above, the objective of the current study is to evaluate the performance of the RIG and STorIT components; thus, direct detection of ions ejected from the STorIT is desired. This measurement was achieved by removing the top CIT end cap and exposing the CIT trapping region to a conversion dynode and electron multiplier tube (EMT) (Model 382, Adaptas Solutions, Palmer, MA) shown in Fig. 1b. High-voltage power supplies (Model PS300, Stanford Research Systems, Sunnyvale, CA) were used to apply +15 V to the bottom CIT end cap and -2450 V to the conversion dynode. The EMT was biased at a voltage of -2250 V which provided an ion signal gain of 6.0×10^7 and facilitated an electrostatic field favorable for ion detection. Ions ejected radially from the STorIT are immediately accelerated towards the conversion dynode due to the potential gradient, creating secondary electrons due to the high energy impact. The signal current from the EMT was fed into a lownoise current pre-amplifier (Model DG645, Stanford Research Systems, Sunnyvale, CA) with a gain of 500 nA/V and an applied 30 kHz low-pass filter. The resulting voltage was fed into a digital oscilloscope (Wavesurfer 3024z, Teledyne LeCroy, Chestnut Ridge, NY) for averaging and recording at a sample rate of 500 kSa/s.

3. Results and discussion

3.1. Ion spectral resolution and trapping capacity

The ion capacity of the STorIT component is an important parameter and vital to the success of the system. To assess the trapping capacity of the STorIT trapping region, mass spectra of xenon were acquired under varying degrees of ionization. Xenon was chosen for this work since it is an inert monoatomic gas with a well characterized isotopic composition, reducing the likelihood of ion-neutral reactions. Xenon gas was introduced into the system at a pressure of 5 μ Torr and a helium pressure of 1.5 mTorr. The RF amplitude was maintained at 750 V_{pp} ($q_z=0.36$) with a $+5.0\,V_{DC}$ offset during ionization (10 ms) and ion cooling (1 ms). Xenon spectra were recorded using a reverse scan with resonance ejection, where the RF was ramped from 750 V_{pp} to 0 V_{pp} in 50 ms. Resonance ejection was achieved by applying a 125 kHz, 700 mV $_{pp}$, and $-350\,$ mV $_{DC}$ offset signal to the AC $_{Tor}$ electrode. The total number of xenon ions trapped within the STorIT was varied by adjusting the filament emission current (10, 20, and 30 μ A) and ionization gate width (5,

6, 7, 8, 9, 10, 15, 20, and 25 ms), for a total of 27 xenon mass spectra acquired for analysis. The results in Fig. 2a show that the total xenon ion population increases with increased ionization. A similar ion signal response was observed by Song et al. when evaluating ion trapping efficiency and trapping capacity of stretched and unstretched RIT devices [32]. Moreover, the total xenon ion population continues to increase at the maximum ionization conditions indicating the STorIT ion trapping capacity is in excess of 2.5x10⁵ xenon ions. For comparison, consider the performance of a RIT presented by Cooks et al. where a trapping volume of 4.0 cm³ ($x_0 = 5$ mm, $y_0 = 4$ mm, L = 50 mm) was found to have a maximum ion capacity of $\sim 6.5 \text{x} 10^4$ ions for a 50 V_{DC} axial potential well [18]. The STorIT device reported here also has an estimated trapping volume of 4.0 cm³, however, toroidal ion traps do not suffer from the bunching of ions near the center of the trap that is encountered with RIT devices. Therefore, a measured ion trapping capacity in excess of 10⁵ ions is consistent with measurements presented in Fig. 2 and highlights the advantages of using a toroidal trapping geometry for ion storage in miniature ion trap systems.

Assessment of the xenon mass spectra recorded under various degrees of ionization is shown in Fig. 2b–d. The mass resolution of xenon ions ejected from the STorIT under low to moderate degrees of ionization typically yielded values $\Delta m=0.5$ –0.6 amu (amu = atomic mass units). These results are reasonably comparable to the mass resolution values for a STorIT device reported by Taylor and Austin [9]. As the ion population increases to $\sim\!2x10^5$ the xenon spectra become slightly broadened; however, several of the xenon isotopes are still resolved. The results in Fig. 2 indicate that the fabricated STorIT device possesses a reasonably high trapping capacity with minimal loss in analytical performance at high ion population conditions.

3.2. Ion trapping efficiency

A key feature of the STorIT system is the ability to store a bulk ion population for sequential mass selective injection into a central CIT for isolated MS² analysis. This requires the STorIT to be able to store ions for an extended period of time. To assess the STorIT's storage efficiency, xenon spectra were acquired for a range of ion storage times following ionization. The intensity of the $^{129}\mathrm{Xe}$ isotope as a function of storage time in Fig. 3a shows that the xenon ion population decays exponentially with increased storage time. There also appears to be a slight dependence on the magnitude of the RF trapping field with a slightly faster ion population decay with higher β_z storage values. Time constants for the observed xenon ion storage times are measured to be 643, 635, and 577 ms for $\beta_z=0.21,\,0.23,\,\mathrm{and}\,0.26,\,\mathrm{respectively}.$

The loss of xenon ion population within the STorIT over time can be partially explained by considering charge exchange reactions occurring within the trapping volume. While these experiments were conducted with xenon sample gas and helium buffer gas, the trap itself was constructed with Delrin and Ultem plastic support structures. These plastics are generally considered suitable for high vacuum applications; however, they do outgas slightly resulting in a small population of neutral hydrocarbon compounds within the RIG and STorIT regions. As a consequence, charge exchange reactions between xenon ions and these

neutral hydrocarbon compounds will result in a measured loss in the total xenon ion population within the STorIT. Charge exchange reactions between xenon ions and neutral hydrocarbons within a QIT have been previously observed by Morand et al. [33]. Evidence of charge exchange reactions within our system is shown in Fig. 3b-d where the collected spectra for 1, 500, and 1750 ms storage times show a clear accumulation of lower mass ions. These spectra show clusters of masses at increments of ~12 amu indicating these ions originate from hydrocarbons. The intensity of these hydrocarbon peaks increases with longer storage times demonstrating that the formation of these ions is kinetically driven as would be expected in a charge exchange reaction. Further evidence of ion loss due to charge exchange reactions is reflected in the dependence on the xenon ion decay time constants and β_z storage values. Higher β_z storage values produce higher xenon ion densities at the trapping center. This increase in reactant density is expected to kinetically accelerate the xenon-hydrocarbon charge exchange reaction rate resulting in the lower storage time constants observed. However, analysis of the xenon and hydrocarbon signals does not account for the loss of trapped xenon ions indicated in Fig. 3a. Therefore, charge exchange reactions are currently considered a minor xenon loss mechanism likely due to the small partial pressure of outgassing hydrocarbon products. We must concede it is also possible charge exchange reactions occur between xenon ions and hydrocarbons with masses below the low-mass-cut-off (LMCO) of the system which is calculated to be m/z =51 at $\beta_z = 0.23$. The creation of these lower mass ions would result in unstable trajectories and would not be observed under the experimental conditions used here.

The coaxial ion trap reported by Peng et al. demonstrated the ability to store and detect ions with negligible signal loss after approximately 6 s of ion storage within the outer toroidal storage ring [30]. The primary difference between the coaxial ion trap reported by Peng et al. and the STorIT system reported here is the shape of the toroidal trapping region. The STorIT device reported here is not a complete toroidal trapping region, rather, is truncated due to the need to increase ion transfer efficiency from the RIG into the STorIT trapping regions as previously discussed. The inclusion of a CIT barrel with slits for ion ejection can also induce small changes to the local trapping field. The unique trapping field and likely enhancement of high-order multipole components at the point where the RIG intersects with the STorIT could potentially lead to the formation of weak local black holes and/or black canyons. Therefore, ions allowed to cool and move throughout the STorIT region could result in losses during long storage durations.

Indeed, more work is required to identify all ion loss mechanisms and improve the trapping efficiency of the STorIT component. However, the device reported here is adequate for the purposes of sequential mass selective sampling from the STorIT region. If we consider the MS^2 analysis of a single component to require $\sim\!50$ ms (transfer time =5 ms, cooling times =5 ms, collision-induced dissociation =10 ms, mass scan =30 ms), approximately five individual mass components could be sampled from the bulk ion population before the ion abundance drops below 50 % of its original population. While this is considered acceptable for the ultimate objective of the proposed SCIT device, further simulation and experimental work on the overall STorIT design

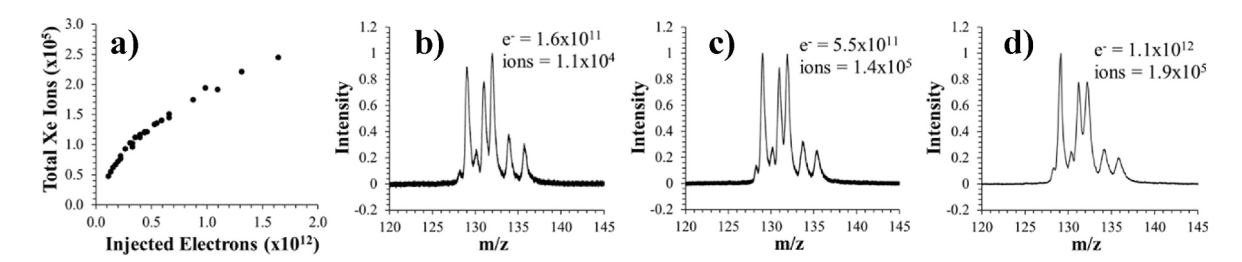


Fig. 2. a) Measured xenon ion population as a function of total injected electrons. b) Xenon mass spectrum for $1.1x10^4$ trapped Xe ions, $\Delta m = 0.55$ amu. c) Xenon mass spectrum for $1.4x10^5$ trapped ions, $\Delta m = 0.56$ amu. d) Xenon mass spectrum for $1.9x10^5$ trapped ions, $\Delta m = 0.81$ amu.

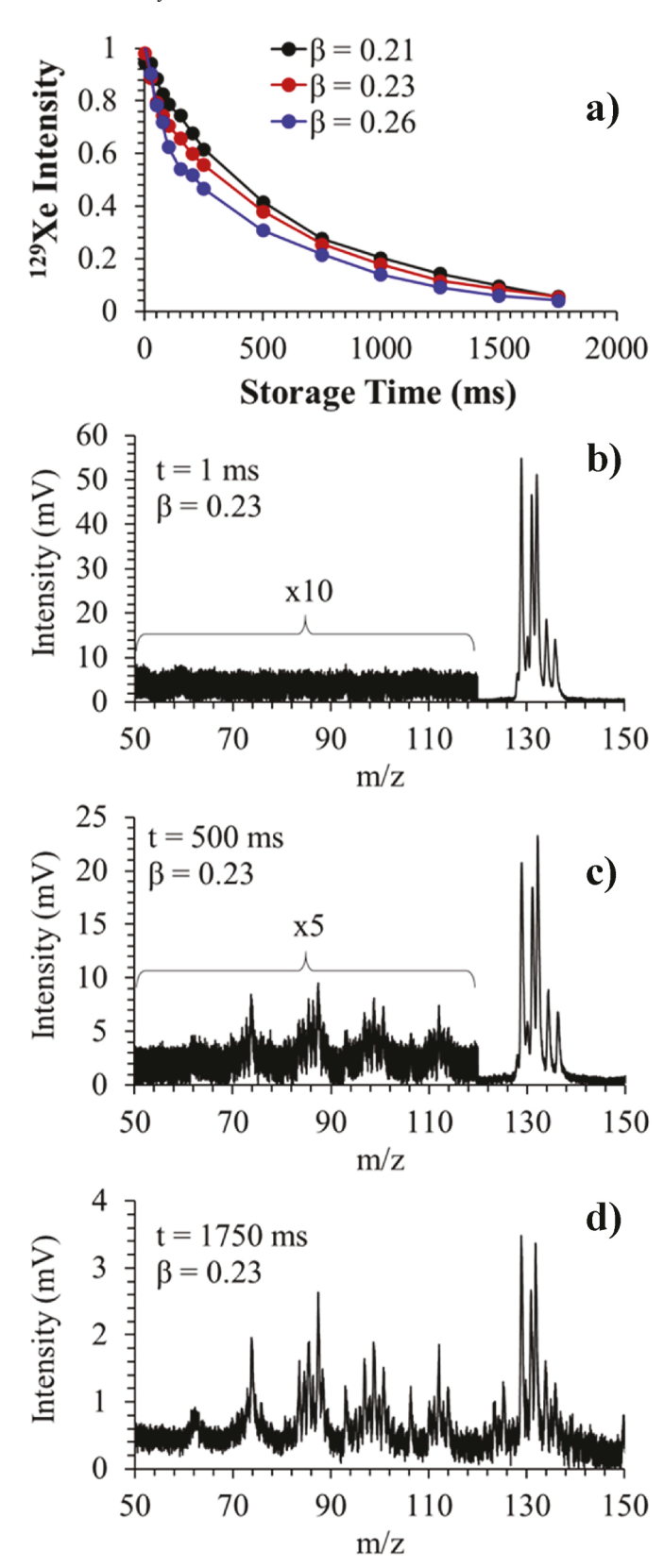


Fig. 3. a) Normalized 129 Xe signal measured as a function of storage time. b) Mass spectrum collected with storage time of 1 ms. c) Mass spectrum collected with a storage time of 500 ms. d) Mass spectrum collected with a storage time of 1750 ms.

including electrode geometry, aspect ratio, and fabrication material is required to improve the overall efficiency of the device.

3.3. Mass spectra of organic compounds

The performance of the RIG and STorIT components was further assessed with the examination of various organic compounds. Mass spectra in Fig. 4a-d were obtained using the previously described reverse RF scan with resonance ejection while the mass spectrum in Fig. 4e was obtained by holding RF = 750 V_{pp} and scanning the AC frequency. The compounds toluene, toluene-D8, and o-xylene were first examined individually by introducing sample vapors into the ionization region at partial pressures $\sim 5~\mu Torr$ with mass spectra shown in Fig. 4a-c. The fragmentation pattern from the ionization of these compounds is consistent with NIST reported mass spectra [34]. Additionally, notable mass peaks at m/z = 105, 114, and 119 for toluene, toluene-D8, and o-xylene, respectively, are larger than the parent ion of each respective compound. A small shoulder peak in the toluene spectra is also observed at m/z = 106. The presence of these mass peaks is the result of gas phase ion-neutral reactions occurring in the trapping region during the ion cooling and mass scan process. In 1974 Shen et al. detailed the toluene reaction as a substitution of a hydrogen atom from a neutral toluene molecule with a CH₂ functional group from an ionized toluene molecule, resulting in the m/z = 105 mass peak observed [35]. Later works by Ausloos and Katritzky et al. confirmed this gas phase toluene reaction [36,37]. Similar reactions occur with toluene-D8 and o-xylene which result in the observed m/z = 114 and 119 mass peaks, respectively. Experimentally, these ion-neutral reactions are moderately favorable within ion trap systems due to the focusing of ions near the trapping center. Ion trap systems examining these organic compounds have routinely reported the observation of the 105, 114, and 119 mass peaks [25,27,28,38,39].

Mass spectra in Fig. 4d and e were acquired from a mixture of toluene, toluene-D8, and o-xylene in a 1.1:1:1 mol ratio, respectively. The mass peaks in these spectra are consistent with the individual mass spectra; however, additional low intensity peaks are observed at m/z=112 and 121. The formation of the m/z=112 peak is the result of neutral toluene-D8 and ionized toluene while the formation of the m/z=121 mass peak is the result of neutral o-xylene and ionized toluene-D8. The results in Fig. 4a–e demonstrate the ability of the STorIT system to mass selectively ejection ions from the toroidal region using resonance ejection.

3.4. Targeted ion ejection

Since the ultimate goal of the STorIT component is to successfully store and mass selectively transfer ions from the STorIT region into the CIT trapping region, it is necessary to demonstrate and characterize the mass selective transfer of ions from the STorIT trapping region into the CIT region. Utilizing the organic mixture noted in Fig. 4, a sample vapor pressure of \sim 5 μ Torr was introduced into the ionization region. The targeted ejection sequence involved 10-ms ionization, 1-ms ion cooling, 5-ms mass selective ejection, and 1-ms ion cooling time, all while RF = 750 V_{pp}. Following ion cooling, a mass spectrum of the remaining ions was acquired using a 50 ms reverse scan with resonance ejection. Several mass spectra were acquired for a range of AC ejection frequencies and four applied AC voltages. The relationship between the selectively ejected mass and applied AC frequency was determined from the data collected in the AC scan in Fig. 4e. Analysis was accomplished by measuring the area under the targeted mass for each acquired spectra. Additionally, several spectra were collected with the targeted ejection frequency tuned to lower masses in order to obtain a baseline signal, allowing the relative mass ejection efficiency to be calculated. The results in Fig. 5a show how the relative population of the m/z = 91ion changes with targeted AC frequency and amplitude. An AC potential of $0.5~V_{pp}$ did not result in appreciable ejection of targeted ions.

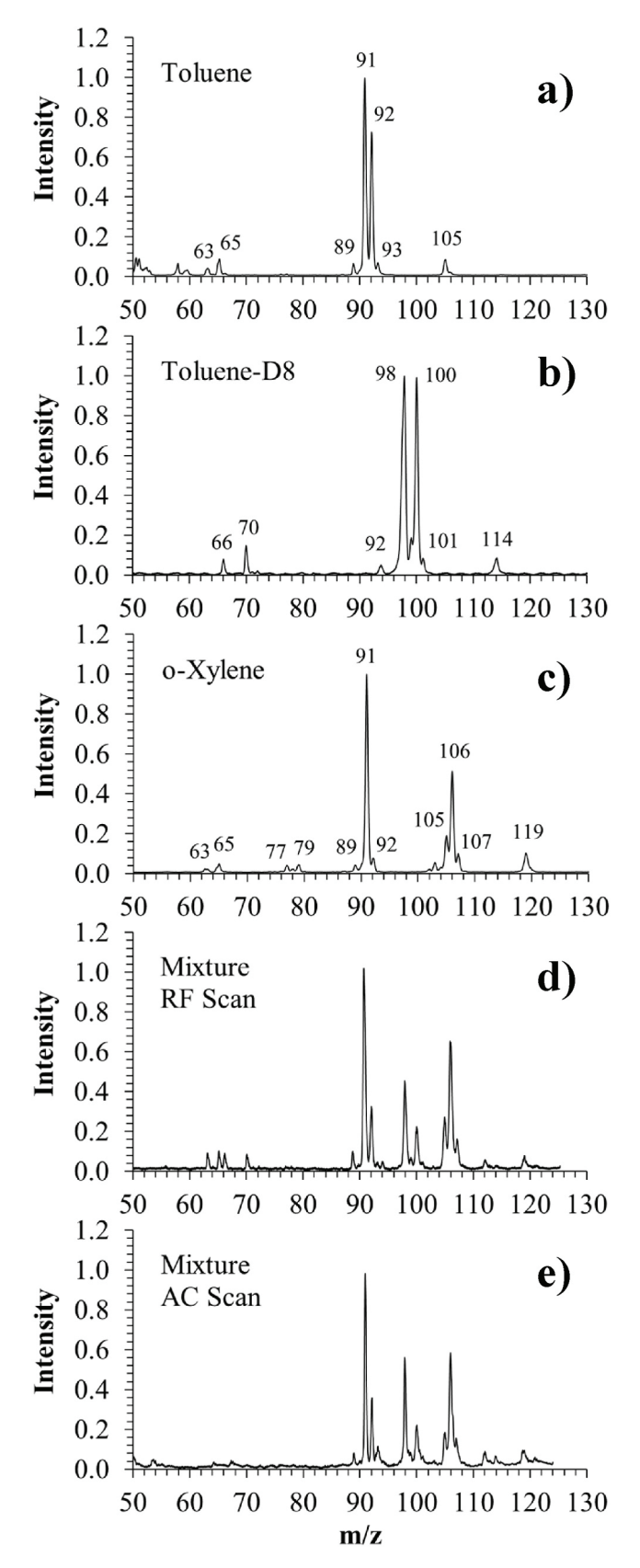


Fig. 4. Mass spectra collected for a) toluene, b) toluene-D8, and c) o-xylene. Mass spectra acquired for a mixture of compounds a-c using d) reverse RF scan with resonance ejections and e) scanning the AC frequency with RF $=750\ V_{pp}$ held constant.

Increasing the AC potential to 1.0 V_{pp} successfully ejects the m/z=91ion with a mass resolution ± 2 amu and an ejection efficiency ~ 87 %. Increasing the AC volage applied to the targeted mass ejection signal further increases the ejection efficiency to ~98 %; however, this also results in a loss in mass selectivity with a resolution of ± 4 amu and ± 7 amu for applied AC potentials of 2.5 V_{pp} and 5.0 V_{pp} , respectively. Fig. 5b shows two mass spectra for an applied AC potential of 2.5 V_{DD} with the targeted ejection frequency tuned off-resonance and tuned to the m/z = 91 ion (on-resonance). A clear population reduction in the m/z = 91z = 91 ion is observed with accompanying reduction in the adjacent m/z= 89 and 92 ions when the targeted AC ejection signal is tuned onresonance. Interestingly, a reduction in the m/z = 105, 112, and 119 ion signals are also observed. Since these ion peaks are the result of ionized toluene reacting with neutral toluene, toluene-D8, and o-xylene, the removal of the reactant toluene ion by targeted ejection suppresses the formation of these methylated products.

A similar result is obtained when targeting the m/z=98 ion as shown in Fig. 5c and d. These data demonstrate that the system can selectively isolate the toluene-D8 compound from the surrounding toluene and oxylene compounds. Additionally, there appears to be a slight reduction in the m/z=107 ion (Fig. 5d). This is consistent with the removal of the toluene-D8 reactant, suppressing the formation of the methylated product. A slight decrease in the m/z=114 and 121 ion signals are also observed.

The parent ion of o-xylene at m/z = 106 was targeted within the mixture with results shown in Fig. 5e and f. These data differ slightly from the m/z = 91 and m/z = 98 targeted data. The application of a 1.0 V_{pp} targeted ejection signal showed a narrow ejection selectivity with an ejection efficiency ~57 %. Small peaks were also observed at m/z = 91and m/z = 100 amu. Increasing the targeted AC potential to 2.5 V_{pp} shows a notable structure that differs from the m/z = 91 and 98 data. Loss of the m/z = 106 ion population is observed when the ejection frequency is tuned from m/z = 87 to m/z = 98 with an ejection efficiency ~29 %. A similar result is found when the targeted ejection signal is increased to 5.0 Vpp, showing a broadening of the targeted mass ejection consistent with the results in Fig. 5a and c. As observed in Fig. 4a, the methylation of neutral toluene from the m/z = 91 toluene ion leads to the formation of m/z = 105 and small levels of m/z = 106. Therefore, the targeted ejection of ions at m/z = 91 suppresses the formation of m/z = 91105 and 106 ions due to the loss of the methylation reactant. When the targeted ejection frequency is tuned to the m/z = 106 ion, an ejection efficiency maximizes at \sim 67 %. This indicates \sim 29 % of the m/z=106ion population is the result of ion-neutral reactions and \sim 67 % of the m/z = 106 ion population originates from the direct ionization of o-xylene. The combination of these ion formation mechanisms accounts for ~96 % of the signal observed at m/z = 106.

The results reported in Fig. 5a–f demonstrate that the constructed device has the ability to mass selectively eject ions from the STorIT region into the CIT with high efficiency and reasonable mass selectivity. These results are consistent with the simulation studies conducted by Gamage et al. which examined the ion transfer efficiency of an m/z=90 ion from a STorIT into a CIT [31].

4. Conclusions

The RIG and STorIT components of a novel SCIT device have been fabricated and experimentally examined. The trapping capacity of the STorIT component was evaluated by varying the number of ionizing electrons injected into the RIG trapping and gas introduction region. The resulting xenon signal was used to calculated the total number of detected ions, and it was found that the STorIT component can successfully store $>2.5 \times 10^5$ ions. Moreover, these results indicate the designed RIG can successfully transfer ions created within the RIG to the STorIT trapping region for analysis. At these high ion populations, the measured xenon spectra showed only a slight diminishment of performance, with typical spectral resolution measured to be between $\Delta m =$

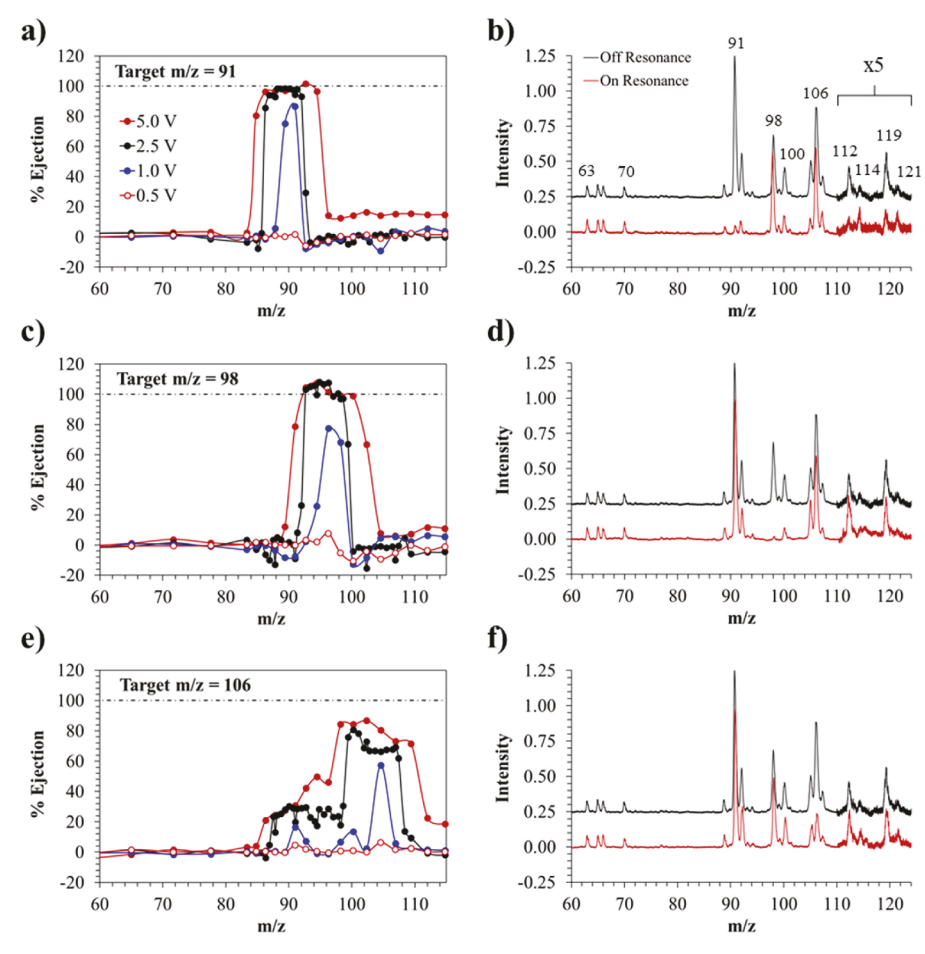


Fig. 5. Measured ejection efficiency as the ejection frequency is incrementally stepped for a) m/z = 91, c) m/z = 98, e) m/z = 106. The applied potential for ion ejections was varied between 0.5, 1.0, 2.5, and 5.0 V_{pp}. Measured spectra collected with a 2.5 V_{pp} AC ejection signal tuned to the targeted mass (on-resonance = red curves) b) m/z = 91, d) m/z = 98, and f) m/z = 106 and tuned away from all mass peaks observed (off-resonance = black curves). Note, the off-resonance spectra have been offset by +0.25 to enhance visual comparison.

0.5–0.6 amu for low to moderate ion populations and rising to $\geq\!0.8$ amu at ion populations above $2x10^5.$ These results demonstrate the STorIT component can successfully store a large ion population with minor degradation in performance.

A primary goal of the STorIT region is to efficiency store ions for sequential mass ejection into a centrally located CIT component for MS² analysis. The trapping efficiency of the RIG and STorIT components was evaluated by varying the storage time of xenon ions trapped within the RIG and STorIT. The currently designed system found the xenon ion population decreases exponentially with increasing ion storage time. The loss of xenon ions is partially due to observed charge exchange reactions occurring between xenon ions and neutral hydrocarbons likely outgassed from plastic structures used to assemble the trap; although, this is considered a minor loss mechanism. Indeed, future SCIT designs would benefit from the use of glass or ceramic components to alleviate this outgassing issue. The primary xenon ion loss mechanism has yet to be identified; however, the unique field formed at the point where the RIG intersects the STorIT may be composed of unfavorable higher order multipole components which could form weak local black holes and/or black canyons resulting in ion loss over long storage durations.

Mass spectra for several organic compounds were also acquired and examined. Toluene, toluene-D8, and o-xylene were first examined individually. Mass spectra using a reverse scan with resonance ejection and an AC frequency sweep were acquired. Mass peaks were observed and are attributed to ion-neutral reactions. From these spectra the STorIT demonstrated the ability to resonantly eject ions from the STorIT trapping region into the CIT trapping region with reasonable mass

resolution

Finally, the STorIT's ability to selectively eject a single mass from a bulk ion population was evaluated. Using the organic compound mixture noted, we showed the STorIT component can selectively eject ions with a mass resolution of ± 2 amu and an ejection efficiency $\sim\!87$ % when a 1.0-V ejection signal was used. Ejection efficiencies near $\sim\!100$ % can be achieved when using the appropriate ejection voltage. It was also demonstrated that larger ion ejection mass windows can be realized by increasing the applied AC voltage. Signals of $2.5~V_{pp}$ and $5.0~V_{pp}$ yielded mass windows of ± 4 and ± 7 amu, respectively, with $\sim\!100$ % ejection efficiency. Future work will focus on characterizing the trapping efficiency of the CIT within the fully assembled SCIT, thus, providing a more complete picture of the overall analytical efficiency of the constructed SCIT device.

We have constructed and successfully demonstrated the analytical utility of the RIG and STorIT components of an SCIT. Studies are currently underway to examine the performance and analytical figures of merit for a fully assembled SCIT device as a gas sampling unit. Future studies will focus on the detection of externally generated ions via paper spray ionization. The work reported is the first of several steps leading to the development of an efficient and versatile miniature SCIT mass analyzer for portable chemical analysis.

CRediT authorship contribution statement

David V. Sirbescu-Stanley: Writing – review & editing, Validation, Methodology, Investigation. **Kristina M. Lemmer:** Writing – review &

editing, Investigation, Formal analysis. **Daniel E. Austin:** Writing – review & editing, Methodology, Formal analysis, Conceptualization. **Nicholas R. Taylor:** Writing – review & editing, Writing – original draft, Visualization, Supervision, Software, Resources, Project administration, Methodology, Investigation, Funding acquisition, Formal analysis, Conceptualization.

Declaration of competing interest

The authors declare the following financial interests/personal relationships which may be considered as potential competing interests:

Nicholas R. Taylor reports financial support was provided by National Science Foundation. If there are other authors, they declare that they have no known competing financial interests or personal relationships that could have appeared to influence the work reported in this paper.

Acknowledgements

The authors would like to thank Kelsey D. Cook and the U.S. National Science Foundation for funding this work (awards 2003667 and 2003592).

Data availability

Data will be made available on request.

References

- W. Paul, H. Steinwedel, A new mass spectrometer without a magnetic field, Z. Naturforsch. 8a (1953) 448–450. https://api.semanticscholar.org/CorpusID: 116267446.
- [2] R.E. March, J.F.J. Todd, Dynamics of ion trapping, in: Quadrupole Ion Trap Mass Spectrom, 2005, pp. 73–132, https://doi.org/10.1002/0471717983.ch3.
- [3] E. Mathieu, Memoire sur le mouvement vibratoire d'une membrane de forme elliptique, J. Math. Pure Appl. 13 (1868) 137.
- [4] R.E. March, An introduction to quadrupole ion trap mass spectrometry, J. Mass Spectrom. 32 (1997) 351–369, https://doi.org/10.1002/(SICI)1096-9888(199704) 32:4<351::AID-JMS512>3.0.CO;2-Y.
- [5] J.C. Schwartz, M.W. Senko, J.E.P. Syka, A two-dimensional quadrupole ion trap mass spectrometer, J. Am. Soc. Mass Spectrom. 13 (2002) 659–669, https://doi. org/10.1016/S1044-0305(02)00384-7.
- [6] S.A. Lammert, W.R. Plass, C. V Thompson, M.B. Wise, Design, optimization and initial performance of a toroidal rf ion trap mass spectrometer, Int. J. Mass Spectrom. 212 (2001) 25–40.
- [7] R.F. Bonner, J.E. Fulford, R.E. March, G.F. Hamilton, The cylindrical ion trap. Part I. General introduction, Int. J. Mass Spectrom. Ion Phys. 24 (1977) 255–269, https://doi.org/10.1016/0020-7381(77)80034-X.
- [8] Z. Ouyang, G. Wu, Y. Song, H. Li, W.R. Plass, R.G. Cooks, Rectilinear ion trap: concepts, calculations, and analytical performance of a new mass analyzer, Anal. Chem. 76 (2004) 4595–4605, https://doi.org/10.1021/ac049420n.
- [9] N. Taylor, D.E. Austin, A simplified toroidal ion trap mass analyzer, Int. J. Mass Spectrom. 321–322 (2012) 25–32, https://doi.org/10.1016/j.ijms.2012.05.011.
- [10] A.N. Kotana, A.K. Mohanty, Determination of multipole coefficients in toroidal ion trap mass analysers, Int. J. Mass Spectrom. 408 (2016) 62–76, https://doi.org/ 10.1016/j.ijms.2016.06.011.
- [11] S.A. Lammert, A.A. Rockwood, M. Wang, M.L. Lee, E.D. Lee, S.E. Tolley, J. R. Oliphant, J.L. Jones, R.W. Waite, Miniature toroidal radio frequency ion trap mass analyzer, J. Am. Soc. Mass Spectrom. 17 (2006) 916–922, https://doi.org/10.1016/j.jasms.2006.02.009.
- [12] A.N. Kotana, A.K. Mohanty, Computation of Mathieu stability plot for an arbitrary toroidal ion trap mass analyser, Int. J. Mass Spectrom. 414 (2017) 13–22, https://doi.org/10.1016/j.ijms.2016.11.021.
- [13] J.M. Higgs, B.V. Petersen, S.A. Lammert, K.F. Warnick, D.E. Austin, Radiofrequency trapping of ions in a pure toroidal potential distribution, Int. J. Mass Spectrom. 395 (2016) 20–26, https://doi.org/10.1016/j.ijms.2015.11.009.
- [14] J.A. Contreras, J.A. Murray, S.E. Tolley, J.L. Oliphant, H.D. Tolley, S.A. Lammert, E.D. Lee, D.W. Later, M.L. Lee, Hand-portable gas chromatograph-toroidal ion trap mass spectrometer (GC-TMS) for detection of hazardous compounds, J. Am. Soc. Mass Spectrom. 19 (2008) 1425–1434, https://doi.org/10.1016/j. iasms.2008.06.022.

- [15] J.M. Higgs, K.F. Warnick, D.E. Austin, Field optimization of toroidal ion trap mass analyzers using toroidal multipoles, Int. J. Mass Spectrom. 425 (2018) 10–15, https://doi.org/10.1016/j.ijms.2017.12.003.
- [16] A. Li, J.M. Higgs, D.E. Austin, Chaotic motion of single ions in a toroidal ion trap mass analyzer, Int. J. Mass Spectrom. (2017), https://doi.org/10.1016/j. iims 2017 06 005
- [17] G. Wu, R.G. Cooks, Z. Ouyang, M. Yu, W.J. Chappell, W.R. Plass, Ion trajectory simulation for electrode configurations with arbitrary geometries, J. Am. Soc. Mass Spectrom. 17 (2006) 1216–1228, https://doi.org/10.1016/j.jasms.2006.05.004.
- [18] Q. Song, S. Kothari, M.A. Senko, J.C. Schwartz, J.W. Amy, G.C. Stafford, R. G. Cooks, Z. Ouyang, Rectilinear ion trap mass spectrometer with atmospheric pressure interface and electrospray ionization source, Anal. Chem. 78 (2006) 718–725, https://doi.org/10.1021/ac0512709.
- [19] Q. Yu, L. Tang, K. Ni, X. Qian, X. Wang, Computer simulations of a new toroidal-cylindrical ion trap mass analyzer, Rapid Commun. Mass Spectrom. 30 (2016) 2271–2278, https://doi.org/10.1002/rcm.7713.
- [20] A.M. Tabert, M.P. Goodwin, J.S. Duncan, C.D. Fico, R.G. Cooks, Multiplexed rectilinear ion trap mass spectrometer for high-throughput analysis, Anal. Chem. 78 (2006) 4830–4838, https://doi.org/10.1021/ac060149e.
- [21] J.D. Maas, P.I. Hendricks, Z. Ouyang, R.G. Cooks, W.J. Chappell, Miniature monolithic rectilinear ion trap arrays by stereolithography on printed circuit board, J. Microelectromech. Syst. 19 (2010) 951–960, https://doi.org/10.1109/ JMEMS 2010 2048554
- [22] S. Kothari, Q. Song, Y. Xia, M. Fico, D. Taylor, J.W. Amy, G. Stafford, R.G. Cooks, Multiplexed four-channel rectilinear ion trap mass spectrometer, Anal. Chem. 81 (2009) 1570–1579, https://doi.org/10.1021/ac8023284.
- [23] P.M. Hettikankanange, D.E. Austin, Varying the aspect ratio of toroidal ion traps: implications for design, performance, and miniaturization, Int. J. Mass Spectrom. 470 (2021) 116703, https://doi.org/10.1016/j.ijms.2021.116703.
- [24] Y. Cheng, Y. Liu, Z. Wu, C. Shen, S. Li, H. Wang, C. Chen, Concept and simulation of a novel dual-layer linear ion trap mass analyzer for micro-electromechanical systems mass spectrometry, Eur. J. Mass Spectrom. (2024) 14690667241251792, https://doi.org/10.1177/14690667241251792.
- [25] Z. Zhang, Y. Peng, B.J. Hansen, I.W. Miller, M. Wang, M.L. Lee, A.R. Hawkins, D. E. Austin, Paul trap mass analyzer consisting of opposing microfabricated electrode plates, Anal. Chem. 81 (2009) 5241–5248, https://doi.org/10.1021/ac9002112.
- [26] D.E. Austin, M. Wang, S.E. Tolley, J.D. Maas, A.R. Hawkins, A.L. Rockwood, H. D. Tolley, E.D. Lee, M.L. Lee, Halo ion trap mass spectrometer, Anal. Chem. 79 (2007) 2927–2932, https://doi.org/10.1021/ac062155g.
- [27] M. Wang, H.E. Quist, B.J. Hansen, Y. Peng, Z. Zhang, A.R. Hawkins, A. L. Rockwood, D.E. Austin, M.L. Lee, Performance of a halo ion trap mass analyzer with exit slits for axial ejection, J. Am. Soc. Mass Spectrom. 22 (2011) 369–378, https://doi.org/10.1007/s13361-010-0027-2.
- [28] B.J. Hansen, R.J. Niemi, A.R. Hawkins, S.A. Lammert, D.E. Austin, A lithographically patterned discrete planar electrode linear ion trap mass spectrometer, J. Microelectromech. Syst. 22 (2013) 876–883, https://doi.org/ 10.1109/JMEMS.2013.2248128.
- [29] A. Li, B.J. Hansen, A.T. Powell, A.R. Hawkins, D.E. Austin, Miniaturization of a planar-electrode linear ion trap mass spectrometer, Rapid Commun. Mass Spectrom. 28 (2014) 1338–1344, https://doi.org/10.1002/rcm.6906.
- [30] Y. Peng, B.J. Hansen, H. Quist, Z. Zhang, M. Wang, A.R. Hawkins, D.E. Austin, Coaxial ion trap mass spectrometer: concentric toroidal and quadrupolar trapping regions, Anal. Chem. 83 (2011) 5578–5584, https://doi.org/10.1021/ac200600u.
- [31] R.W. Gamage, P.M. Hettikankanange, K.D. Lyman, D.E. Austin, N.R. Taylor, Simplified coaxial ion trap: simulation-based geometry optimization, unidirectional ejection, and trapping conditions, Int. J. Mass Spectrom. 474 (2022) 116801, https://doi.org/10.1016/j.ijms.2022.116801.
 [32] Y. Song, G. Wu, Q. Song, R.G. Cooks, Z. Ouyang, W.R. Plass, Novel linear ion trap
- [32] Y. Song, G. Wu, Q. Song, R.G. Cooks, Z. Ouyang, W.R. Plass, Novel linear ion trap mass analyzer composed of four planar electrodes, J. Am. Soc. Mass Spectrom. 17 (2006) 631–639, https://doi.org/10.1016/j.jasms.2005.12.014.
- [33] K.L. Morand, S.R. Horning, R.G. Cooks, A tandem quadrupole-ion trap mass spectrometer, Int. J. Mass Spectrom. Ion Process. 105 (1991) 13–29, https://doi. org/10.1016/0168-1176(91)85085-Z.
- [34] W.E. Wallace, Mass spectra, in: P.J. Linstrom, W.G. Mallard (Eds.), NIST Chem. WebBook, NIST Stand. Ref. Database Number 69, National Institute of Standards and Technology, Gaithersburg MD 20899 (Retrieved July 23, 2024).
- [35] J. Shen, R.C. Dunbar, G.A. Olah, Gas phase benzyl cations from toluene precursors, J. Am. Chem. Soc. 96 (1974) 6227–6229.
- [36] P. Ausloos, Structure and isomerization of C7H7+ ions formed in the charge-transfer-induced fragmentation of ethylbenzene, toluene, and norbornadiene, J. Am. Chem. Soc. 104 (1982) 5259–5265.
- [37] A.R. Katritzky, Z. Dega-Szafran, R. Ramanathan, J.R. Eyler, Ion cyclotron resonance mass spectrometric study of ion—molecule reactions in toluene—pyridine mixtures, Org, Mass Spectrom. 29 (1994) 96–101.
- [38] Y. Tian, T.K. Decker, J.S. McClellan, L. Bennett, A. Li, A. De la Cruz, D. Andrews, S. A. Lammert, A.R. Hawkins, D.E. Austin, Improved miniaturized linear ion trap mass spectrometer using lithographically patterned plates and tapered ejection slit, J. Am. Soc. Mass Spectrom. (2017), https://doi.org/10.1007/s13361-017-1759-z.
 [39] J. Moxom, P.T.A. Reilly, W.B. Whitten, J.M. Ramsey, Analysis of volatile organic
- [39] J. Moxom, P.T.A. Reilly, W.B. Whitten, J.M. Ramsey, Analysis of volatile organic compounds in air with a micro ion trap mass analyzer, Anal. Chem. 75 (2003) 3739–3743, https://doi.org/10.1021/ac034043k.